Version of Record: https://www.sciencedirect.com/science/article/pii/S0022509620301538
Manuscript_93b7899d57c0b504b8e061bd969cdf35

Ductile failure as a constitutive instability in porous plastic solids

S. M. Keralavarma[a], D. Reddi[a], A. A. Benzerga[b,c]
[a]**Department of Aerospace Engineering, Indian Institute of Technology Madras**
Chennai 600036, India
[b]**Department of Aerospace Engineering, Texas A&M University**
College Station, TX 77843-3141, USA
[c]**Department of Materials Science & Engineering, Texas A&M University**
College Station, TX 77843-3141, USA

Abstract

A criterion for ductile rupture is derived using Rice's theory for macroscopic strain localization, and a constitutive relation for porous plastic solids that accounts for inhomogeneous yielding at the mesoscale. At the microscopic scale, it is assumed that failure occurs by void coalescence along a band of voids. An approximate, parameter-free closed form expression for the failure criterion is derived as a function of a single scalar damage variable –the porosity– and the macroscopic stress state, characterized by the stress triaxiality and Lode parameters. For practical applications, an uncoupled approach is developed whereby the failure criterion is supplemented with a damage-free plasticity model and a loading path dependent damage evolution law. The predictive capabilities of the approach are illustrated by comparisons with finite element cell model studies. In particular, the influence of strain hardening is investigated in some detail.

1. Introduction

Whether ductile failure occurs by instability or by the impingement of void-like defects has long been debated (Needleman and Rice, 1978; Tekoğlu et al., 2015). It would be fair to state that, for most practical cases, the answer is still unknown, and may be scale-dependent. Plastic instability may follow from a variety of mechanisms, some of which do not involve microvoids (Benzerga et al., 2019). The focus of this paper is on void-mediated ductile failure. Under such circumstances, when failure occurs subsequent to a plastic instability, a key question is that of what constitutive relation best represents the behavior of the material at hand, which is *de facto* porous, up to the point of macroscopic strain localization (Rice, 1976).

The behavior of porous plastic solids has been analyzed from first principles by considering elementary cells subjected to mesoscopically *homogeneous* deformation, along with the theory of limit analysis for rigid–plastic bodies (Gurson, 1977; Benzerga and Leblond, 2010; Madou and Leblond, 2012). In this class of models, the locations $\underline{x}$ of surface points, originally having locations $\underline{X}$, are prescribed as: $\underline{x} = \mathbf{F}\underline{X}$ with $\mathbf{F}$ spatially constant, obviously to be interpreted as the mesoscopic deformation gradient. By definition, such boundary conditions preclude strong strain concentrations within the cell, as would arise should elastic unloading occur in parts of the cell (Koplik and Needleman, 1988). This essential limitation of Gurson-like models can be relaxed by employing

boundary conditions that allow for mesoscopically *inhomogeneous* deformation, such as periodic boundary conditions. This is precisely what has been achieved in more recent analyses, initiated by Benzerga and Leblond (2014) and further developed by others; see Keralavarma and Chockalingam (2016) and references therein. This new class of models represents the potentially inhomogeneous yielding of porous solids.

The significance of inhomogeneous yielding models is obvious. First, the strain softening inherent to these models can be orders of magnitude larger than models that assume homogeneous yielding, such as Gurson's. This in itself may lead to macroscopic strain localization under circumstances where the porosity-induced softening of homogeneous yielding models would still be subcritical. Alternatively, in an evolution problem, the transition from homogeneous to inhomogeneous yielding may lead to an abrupt drop in the load carrying capacity thus leading to fracture before localization even sets in. Furthermore, inhomogeneous yielding may set in while the global response does not exhibit any softening, as recently studied by Torki and Benzerga (2018) for shear-dominated loadings.

The connection between void coalescence and strain localization was recently discussed by Morin et al. (2016) (see their Appendix A). Coalescence has often been interpreted as a localization occurring at the scale of some homogenized model of porous material plasticity. Perrin (1992) investigated this by applying the results of Rudnicki and Rice (1975) on localization in pressure-sensitive materials, as specialized by Yamamoto (1978), to Gurson's constitutive relation. He found that Gurson's model did predict strain localization within planar layers parallel to the intervoid ligaments, in agreement with the cell model studies of Koplik and Needleman (1988), but for values of the porosity far greater than those reported by these authors at the onset of coalescence. One interpretation of this failure, put forth by Morin et al. (2016), is that the Gurson model does not account for inhomogeneous yielding.

More recently, Reddi et al. (2019) have combined the Gurson model and an isotropic version of the void coalescence model proposed by Keralavarma and Chockalingam (2016) into a multisurface model of porous material plasticity. Even more recently, Vishwakarma and Keralavarma (2019) have carried out a preliminary strain localization analysis on the multi-surface model along with three-dimensional cell model analyses. They found that the strain to the onset of coalescence in the cell model simulations correlates well with the strain at which plastic instability is predicted using the criterion of Rice (1976). In addition, the orientation of the localization plane coincided approximately with the orientation of the planar band along which void coalescence was predicted by the multi-surface model (see Fig.16 of Vishwakarma and Keralavarma, 2019). Thus, the development of inhomogeneous yielding models presents perspectives for addressing the question at hand, in a fundamental way.

An equally important question is how to account for the influence of strain-hardening, which plays a key role in localization phenomena. Currently available models of void coalescence, or more generally of inhomogeneous yielding, are based on classical limit analysis for ideally plastic solids. The chief concern of this paper is to carry out a strain-localization analysis assuming a constitutive relation that accounts for (i) inhomogeneous yielding, and (ii) strain hardening; the latter being introduced using a variant of Gurson's heuristics.

From a practical standpoint, the instability-based failure criterion is shown to bear a closed-form expression suitable for structural computations. The developed criterion is

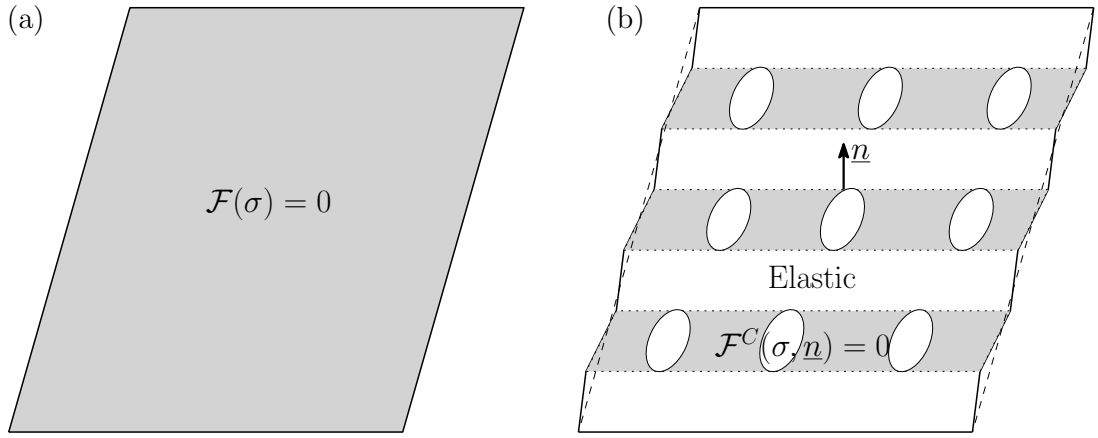

Figure 1: Alternative modes of yielding of a porous elementary cell by (a) homogeneous yielding (diffuse plasticity) and (b) inhomogeneous yielding along planar bands with normal, $\underline{n}$.

neither of the critical-strain type nor of the critical internal-state-variable type, although it may be cast in either form under special types of loading. Thus, in the second part of the paper, the criterion is supplemented with a damage-free plasticity model along with a heuristic damage evolution equation, within an uncoupled approach, so as to enable direct comparisons with finite-element micromechanical computations. Uncoupled plasticity and damage growth models are frequently used to model ductile failure by void growth to coalescence in metals (Pineau et al., 2016). Classical models of this kind, such as the Beremin (1981) or Johnson and Cook (1985) models, are based on the Rice and Tracey (1969) equation for the growth of isolated voids under remote axisymmetric loading. In particular, they do not account for the influence of shear on the critical conditions for fracture initiation.

2. Formulation

2.1. Plastic constitutive relation

Inhomogeneous yielding refers to a mode of deformation inside a porous cell such that the plastic strain concentrates along bands of voids, as shown schematically in Fig. 1 for the case of shear-dominated loading. The process of void coalescence begins when the mode of yielding changes from diffuse throughout the matrix to concentrated within the inter-void ligaments. This type of strain concentration is different from strain localization in the sense of Rice (1976) which implies infinite concentrations.

For simplicity, focus is laid on isotropic response so that every orientation is a potential one for coalescence. The (orientation-dependent) effective yield criterion for inhomogeneous yielding developed by Keralavarma and Chockalingam (2016) reads:

$$\mathcal{F}^C(\boldsymbol{\sigma}, \underline{n}) := 3\frac{\sigma_{\rm sh}^2}{\bar{\sigma}_b^2} + 2f_b \cosh\left(\beta(f_b)\frac{\sigma_{\rm n}}{\bar{\sigma}_b}\right) - 1 - f_b^2 = 0 \tag{1}$$

where $\underline{n}$ denotes the unit vector normal to the band of concentrated strain, $\sigma_{\rm n} = \underline{n} \cdot \boldsymbol{\sigma}\underline{n}$ and $\sigma_{\rm sh} = \sqrt{\underline{n} \cdot \boldsymbol{\sigma}^2\underline{n} - \sigma_{\rm n}^2}$ are, respectively, the normal and shear stresses resolved in the band (smeared to a plane in the continuum description) and f_b is the porosity inside the band. Also, $\bar{\sigma}_b$ is an "average" flow stress of the matrix inside the band, which is in general larger than the average flow stress $\bar{\sigma}$ in the entire cell due to the inhomogeneity of

plastic flow and strain hardening around the voids[1]. The parameter β in (1) is a function of f_b:

$$\beta(f_b) = \sqrt{\frac{5}{6}} \ln\left(\frac{1}{f_b}\right) \left[\sqrt{b^2+1} - \sqrt{b^2+f_b^2} + b \ln\left(\frac{b+\sqrt{b^2+f_b^2}}{f_b(b+\sqrt{b^2+1})}\right)\right]^{-1} \tag{2}$$

with b given by

$$b = \sqrt{\frac{1}{3} + \frac{5}{288}\frac{1}{f_b}(1+f_b-5f_b^2+3f_b^3)} \tag{3}$$

In a statistically isotropic porous material with equiaxed and randomly distributed voids, the orientation of the band normal vector $\underline{n}$ is determined solely by the state of stress. Assuming a band thickness equal to the void size (Benzerga, 2002), f_b is approximately related to the overall porosity as $f_b = f^{2/3}$. The orientation of the strain concentration band is determined by minimizing the effective yield stress or, equivalently, maximizing the value of the yield function $\mathcal{F}^C(\boldsymbol{\sigma}, \underline{n})$, over all possible orientations $\underline{n}$. Keralavarma (2017) showed that the unit vector, $\underline{n}^c$, that maximizes $\mathcal{F}^C(\boldsymbol{\sigma}, \underline{n})$ must be either an eigenvector of $\boldsymbol{\sigma}$ or a linear combination of two eigenvectors corresponding to unequal principal stresses. In the former case, coalescence occurs by internal necking of the ligaments along a band aligned with the major principal plane, when the normal stress satisfies criterion (1). In the latter case coalescence occurs under combined tension and shear of the ligaments along a band whose normal vector is generally found to lie on the plane defined by the maximum and minimum principal stress for realistic values of the porosity ($f \sim \mathcal{O}(0.1)$ or smaller).

Therefore, an *isotropic* coalescence criterion is given by $\mathcal{F}^{C^{\text{iso}}}(\boldsymbol{\sigma}) := \mathcal{F}^C(\boldsymbol{\sigma}, \underline{n}^c) = 0$, where $\underline{n}^c$ is viewed as an isotropic function of $\boldsymbol{\sigma}$, determined as above. Let $s_1 \geq s_2 \geq s_3$ denote the ordered set of principal values of the normalized stress tensor $\mathbf{s} := \boldsymbol{\sigma}/\sigma_{\text{eq}}$, and $\underline{n}^1, \underline{n}^2, \underline{n}^3$ denote the corresponding principal directions. Here, $\sigma_{\text{eq}} := \sqrt{\frac{3}{2}\boldsymbol{\sigma}' : \boldsymbol{\sigma}'}$ denotes the von Mises equivalent stress where $\boldsymbol{\sigma}'$ is the stress deviator. Introducing the stress triaxiality, T, and the Lode parameter, L, as

$$T := \frac{\sigma_{\text{m}}}{\sigma_{\text{eq}}}, \qquad L := -\frac{27}{2}\det\left(\frac{\boldsymbol{\sigma}'}{\sigma_{\text{eq}}}\right) \tag{4}$$

with $\sigma_{\text{m}} = \frac{1}{3}\text{tr}(\boldsymbol{\sigma})$, the normalized principal stresses can be rewritten as:

$$s_1 = T + \frac{2}{3}\cos\theta, \quad s_2 = T - \frac{2}{3}\cos\left(\theta + \frac{\pi}{3}\right), \quad s_3 = T - \frac{2}{3}\cos\left(\theta - \frac{\pi}{3}\right) \tag{5}$$

where $\theta := \frac{1}{3}\cos^{-1}(-L)$ is the so called Lode angle. By definition, $\theta \in \left[0, \frac{\pi}{3}\right]$, so that the condition $s_1 \geq s_2 \geq s_3$ is satisfied. Assuming that the vector $\underline{n}^c$ lies in the $\underline{n}^1 - \underline{n}^3$ plane,

[1] In fact, Keralavarma and Chockalingam (2016) assumed $\bar{\sigma}_b = \bar{\sigma}$, which is true when the first transition occurs from diffuse to concentrated plasticity in the ligaments. However, it is observed in cell model simulations that strain hardening in the ligaments can lead to the cell reverting to a diffuse mode of yielding, such that when void coalescence occurs at higher strain levels, the average plastic strain in the ligaments can be higher than the average for the entire cell.

$\mathcal{F}^{C^{\text{iso}}}(\boldsymbol{\sigma})$ can be expressed in the following approximate, yet accurate form (Reddi et al., 2019)

$$\mathcal{F}^{C^{\text{iso}}}(\boldsymbol{\sigma}) = 3c_{\text{sh}}^2 \left(\frac{\sigma_{\text{eq}}}{\bar{\sigma}_b}\right)^2 + 2f_b \cosh\left(\beta c_{\text{n}} \frac{\sigma_{\text{eq}}}{\bar{\sigma}_b}\right) - 1 - f_b^2 \tag{6}$$

where c_{n} and c_{sh} are the values of the normal and shear stresses on the plane perpendicular to $\underline{n}^c$, normalized by the Mises stress σ_{eq}, given by

$$c_{\text{n}} = (1+\eta)\frac{s_1+s_3}{2}, \qquad c_{\text{sh}} = \left[\left(\frac{s_1-s_3}{2}\right)^2 - \eta^2\left(\frac{s_1+s_3}{2}\right)^2\right]^{1/2} \tag{7}$$

and the parameter η is given by

$$\eta = \min\left\{\frac{f_b\beta^2}{3-f_b\beta^2}, \left|\frac{s_1-s_3}{s_1+s_3}\right|\right\} \tag{8}$$

The unit vector $\underline{n}^c$ that maximizes $\mathcal{F}^C(\boldsymbol{\sigma}, \underline{n})$ is given by

$$\underline{n}^c = \sqrt{\frac{1}{2}\left[1+\eta\frac{s_1+s_3}{s_1-s_3}\right]}\underline{n}^1 + \sqrt{\frac{1}{2}\left[1-\eta\frac{s_1+s_3}{s_1-s_3}\right]}\underline{n}^3 \tag{9}$$

Notice that, at sufficiently large stress triaxialities when $|s_1-s_3| \ll |s_1+s_3|$, $\underline{n}^c$ approaches the direction of the maximum absolute principal stress $\underline{n}^1$ or $\underline{n}^3$; i.e. coalescence occurs by internal necking in the absence of shear. At lower triaxialities and realistic porosities, it is found that $\eta = f_b\beta^2/(3-f_b\beta^2) \ll 1$, so that the angle between $\underline{n}^c$ and the major principal direction $\underline{n}^1$ will be close to 45° on the $\underline{n}^1 - \underline{n}^3$ plane; and coalescence occurs under combined tension and shear.

Plastic flow post the onset of coalescence is governed by the normality flow rule

$$\mathbf{d}^p = \dot{\lambda}\mathbf{N}, \qquad \mathbf{N} = \frac{\partial \mathcal{F}^{C^{\text{iso}}}}{\partial \boldsymbol{\sigma}} \tag{10}$$

where $\mathbf{d}^p$ is the Eulerarian rate of plastic deformation, $\mathbf{N}(\boldsymbol{\sigma})$ is the flow direction tensor normal to the yield surface, and $\dot{\lambda}$ is the plastic multiplier. Since the isotropic yield surface $\mathcal{F}^{C^{\text{iso}}}(\boldsymbol{\sigma}) = 0$ is the envelope of the family of surfaces defined parametrically by $\mathcal{F}^C(\boldsymbol{\sigma}, \underline{n}) = 0$, with $\underline{n}$ as the parameter, $\mathcal{F}^{C^{\text{iso}}}(\boldsymbol{\sigma}) = \mathcal{F}^C(\boldsymbol{\sigma}, \underline{n}^c)$ at any point on the isotropic yield surface, where $\underline{n}^c$ is the value of $\underline{n}$ that extremizes $\mathcal{F}^C(\boldsymbol{\sigma}, \underline{n})$; see Eq.(9). Further, the normal to a level surface of $\mathcal{F}^{C^{\text{iso}}}(\boldsymbol{\sigma})$ will be collinear with the normal to the corresponding level surface of $\mathcal{F}^C(\boldsymbol{\sigma}, \underline{n}^c)$. Hence, one can also write

$$\mathbf{N} = \frac{\partial \mathcal{F}^C}{\partial \boldsymbol{\sigma}}(\boldsymbol{\sigma}, \underline{n}^c) \tag{11}$$

Strain hardening is specified by writing the yield stress in the band $\bar{\sigma}_b$ as a monotonically increasing function of a work conjugate 'effective' plastic strain in the band, ε_b^p; i.e. $\bar{\sigma}_b = \bar{\sigma}_b(\varepsilon_b^p)$. The rates of evolution of the internal variables in the model, ε_b^p and f, can be written in the form

$$\dot{\varepsilon}_b^p = \dot{\lambda}Q_p, \qquad \dot{f} = \dot{\lambda}Q_f \tag{12}$$

where the expressions for Q_p and Q_f are obtained in the usual way by equating the microscopic and mesoscopic rates of plastic work and by requiring mass conservation, respectively. The resulting expressions read (Vishwakarma and Keralavarma, 2019)

$$Q_p = \frac{\boldsymbol{\sigma} : \mathbf{N}}{f(1/f_b - 1)\bar{\sigma}_b} \qquad Q_f = (1-f)\mathrm{tr}(\mathbf{N}) \tag{13}$$

Note that, unlike the expression for Q_f, which is rigorous to the neglect of elasticity, the above expression for Q_p is not rigorous. Rather, it is based on heuristics first introduced by Gurson (1977), which assumes the existance of a fictitious homogeneously deforming material of volume equal to the volume of plastically deforming material in the RVE, whose rate of dissipation equals that of the entire RVE. For a rate independent material, the plastic multiplier $\dot{\lambda} \geq 0$ is obtained from the consistency condition $\dot{\lambda}\dot{\mathcal{F}}^C = 0$.

2.2. Localization analysis

According to Rice's criterion, failure by plastic instability occurs when the determinant of the acoustic tensor

$$\mathbf{A}(\underline{n}) := \underline{n} \cdot \mathbb{C}^t \cdot \underline{n}, \tag{14}$$

with $\mathbb{C}^t$ the elasto-plastic tangent modulus, vanishes for any material plane with unit normal $\underline{n}$. The expression for $\mathbb{C}^t$ depends on the plastic constitutive behavior of the material at the onset of instability. Recent analysis using a multi-surface model, which accounted for the competition between homogeneous yielding of a porous material accoring to the Gurson (1977) criterion, and inhomogeneous yielding using criterion (6), showed that the above instability condition is always satisfied after the onset of coalescence, irrespective of the loading path (Vishwakarma and Keralavarma, 2019). Further, the orientation of the localization plane $\underline{n}$ is predicted to be nearly identical to the coalescence plane $\underline{n}^c$ (see Fig.16 in Vishwakarma and Keralavarma, 2019). Therefore, we adopt the criterion

$$\det\left(\mathbf{A}(\underline{n}^c)\right) = 0 \tag{15}$$

to determine failure by localization instability using $\underline{n} \approx \underline{n}^c$ from equation (9).

The elasto-plastic tangent modulus $\mathbb{C}^t$ evaluates to

$$\mathbb{C}^t = \mathbb{C} - \frac{1}{\mathcal{D}}(\mathbb{C}\mathbf{N}) \otimes (\mathbb{C}\mathbf{N}), \qquad \mathcal{D} := \mathbf{N} : \mathbb{C}\mathbf{N} - \frac{\partial \mathcal{F}^C}{\partial \bar{\sigma}_b} H(\varepsilon_b^p) Q_p - \frac{\partial \mathcal{F}^C}{\partial f} Q_f \tag{16}$$

where $\mathbf{N}$ is the plastic flow direction tensor during inhomogeneous yielding, given by (11), $\mathbb{C}$ is the elastic stiffness tensor and $H(\varepsilon_b^p) = \partial\bar{\sigma}_b/\partial\varepsilon_b^p$ is the instantaneous strain hardening rate in the coalescence band. Using (1) in (11), the tensor $\mathbf{N}$ can be expressed in the following form

$$\mathbf{N} = \mathcal{N}\underline{n}^c \otimes \underline{n}^c + \frac{1}{2}\mathcal{S}(\underline{m}^c \otimes \underline{n}^c + \underline{n}^c \otimes \underline{m}^c), \qquad \underline{m}^c := \frac{\boldsymbol{\sigma}\underline{n}^c - \sigma_{\mathrm{n}}\underline{n}^c}{|\boldsymbol{\sigma}\underline{n}^c - \sigma_{\mathrm{n}}\underline{n}^c|} \tag{17}$$

where $\underline{m}^c$ is a unit vector along the direction of shear stress on the plane of coalescence, and $\mathcal{N}$ and $\mathcal{S}$ are given by

$$\mathcal{N} := \frac{\partial \mathcal{F}^C}{\partial \sigma_{\mathrm{n}}} = \frac{2\beta f_b}{\bar{\sigma}_b} \sinh\left(\beta c_{\mathrm{n}} \frac{\sigma_{\mathrm{eq}}}{\bar{\sigma}_b}\right), \qquad \mathcal{S} := \frac{\partial \mathcal{F}^C}{\partial \sigma_{\mathrm{sh}}} = \frac{6 c_{\mathrm{sh}} \sigma_{\mathrm{eq}}}{\bar{\sigma}_b^2} \tag{18}$$

Recall that the parameters $c_{\rm n}$ and $c_{\rm sh}$ are functions of the loading parameters T and L via Eqs. (7) and (5). Eq.(17) represents the general form of tensor $\mathbf{N}$ when plastic flow is localized into planar bands at the meso-scale, as illustrated in Fig. 1(b). The uniaxial deformation mode observed during void coalescence by internal necking in axisymmetric cell model simulations is a special case of (17) corresponding to $\mathcal{S} = 0$.

Simplified expressions for the terms Q_p and Q_f appearing in $(16)_2$ can be obtained by substituting $(17)_1$ in (13), yielding

$$Q_p = \frac{(\mathcal{N}c_{\rm n} + \mathcal{S}c_{\rm sh})}{f(1/f_b - 1)}\frac{\sigma_{\rm eq}}{\bar{\sigma}_b}, \qquad Q_f = (1-f)\mathcal{N} \tag{19}$$

Using $(17)_1$ and $(16)_1$ in (14), and assuming isotropic elasticity with $\mathbb{C} = 2\mu\mathbb{I}^s + \lambda\mathbf{I}\otimes\mathbf{I}$, where $\mathbb{I}^s$ and $\mathbf{I}$ are the symmetric fourth and second order identity tensors respectively, and λ and μ are the Lamé constants, the acoustic tensor $\mathbf{A}(\underline{n}^c)$ evaluates to

$$\mathbf{A}(\underline{n}^c) = \mu\mathbf{I} - \frac{1}{\mathcal{D}}\mu^2\mathcal{S}^2\underline{m}^c\otimes\underline{m}^c + \left[(\lambda+\mu) - \frac{1}{\mathcal{D}}(\lambda+2\mu)^2\mathcal{N}^2\right]\underline{n}^c\otimes\underline{n}^c - \frac{1}{\mathcal{D}}\mu(\lambda+2\mu)\mathcal{N}\mathcal{S}(\underline{m}^c\otimes\underline{n}^c + \underline{n}^c\otimes\underline{m}^c) \tag{20}$$

Calculating the determinant of the above tensor, we obtain

$$\det\left(\mathbf{A}(\underline{n}^c)\right) = \frac{1}{\mathcal{D}}\mu^2(\lambda+2\mu)\left[\mathcal{D} - \mu\mathcal{S}^2 - (\lambda+2\mu)\mathcal{N}^2\right] \tag{21}$$

Using $(17)_1$ in $(16)_2$ yields

$$\mathcal{D} = \mu\mathcal{S}^2 + (\lambda+2\mu)\mathcal{N}^2 - \frac{\partial\mathcal{F}^C}{\partial\bar{\sigma}_b}H(\varepsilon_b^p)Q_p - \frac{\partial\mathcal{F}^C}{\partial f}Q_f \tag{22}$$

On account of (21) and (22), the strain localization criterion (15) takes the form:

$$\mathcal{C}(T,L,f) := -\frac{\partial\mathcal{F}^C}{\partial\bar{\sigma}_b}H(\varepsilon_b^p)Q_p - \frac{\partial\mathcal{F}^C}{\partial f}Q_f = 0 \tag{23}$$

which turns out to be independent of the elastic constants. In fact, the above-defined function $\mathcal{C}$ is proportional to the plastic hardening modulus (parameter h in Rudnicki and Rice, 1975; Rice, 1976), so that the localization criterion amounts to vanishing hardening modulus. Localization criteria for several other plasticity models reduce to the above form, independent of the elastic constants, when normality is satisfied and the intermediate principal value of the plastic flow direction tensor $\mathbf{N}$ vanishes, as in the case of the present model (see Rice, 1976, Sections 3.3–3.4 for examples). In addition to T, L and f, the terms in Eq.(23) also depend on $\sigma_{\rm eq}$ and $\bar{\sigma}_b$, which will be specified in the next section.

2.3. Uncoupled model of ductile failure

The format of the localization criterion clearly shows that failure is determined by the competition between strain hardening in the coalescence band (first term) and the softening due to void growth in the band (second term). Since the localization indicator $\mathcal{C}(T,L,f)$ is a monotonically decreasing function of the porosity f, the criterion

$$\mathcal{C}(T,L,f) \le 0 \tag{24}$$

could be used to check for 'failure' of a material element in a plasticity simulation. The underlying assumption is that the onset of localization is quickly followed by complete material failure, so that the plastic strain at the onset of localization represents an accurate lower bound measure of the failure strain.

Loading history dependence is implicit in Eq.(23) through the values of the equivalent stress σ_{eq}, the flow stress in the localization band $\bar{\sigma}_b$ and the porosity f. These are determined by (i) the pre-localization plasticity model, (ii) the effect of strain hardening in the coalescence band, and (iii) the evolution law for the porosity, respectively. They are specified in order in what follows.

2.3.1. Pre-localization plasticity model

We adopt an uncoupled approach whereby the elasto-plastic behavior of the material is assumed to be independent of the damage variable –the porosity– prior to localization. For simplicity, we use the rate independent J_2 flow theory with the yield criterion

$$\mathcal{F}(\boldsymbol{\sigma}) := \sigma_{\text{eq}} - \bar{\sigma} = 0 \tag{25}$$

and the plastic deformation rate $\mathbf{d}^p$ given by the associated flow rule. Accordingly, the von Mises equivalent stress σ_{eq} equals the material flow stress $\bar{\sigma}$, which can be written as an arbitrary monotonically increasing function of the scalar equivalent plastic strain, $\varepsilon^p_{\text{eq}}$, assuming isotropic hardening:

$$\bar{\sigma} = \bar{\sigma}(\varepsilon^p_{\text{eq}}), \qquad \varepsilon^p_{\text{eq}} := \int_0^t \sqrt{\frac{2}{3}\mathbf{d}^p : \mathbf{d}^p}\, \mathrm{d}t \tag{26}$$

where t denotes a time-like quantity. Note that, due to the choice of the uncoupled approach and the J_2 plasticity model, the value of σ_{eq} can be written as an explicit function of the plastic strain, independent of the loading history. However, the value of σ_{eq} becomes history dependent for other choices of the pre-localization plasticity model, such as coupled damage-plasticity models.

2.3.2. Strain hardening in the band

Homogenized models of porous plasticity, such as (1), are derived using limit analysis, which assumes ideal plastic behavior for the matrix. Therefore, heuristic approaches are necessary to account for the effect of strain hardening, such as the energy based method proposed by Gurson (1977). In the present case, the observation from coupled damage-plasticity analysis that the onset of macroscopic instability, in the sense of Rice, is predicted immediately after the onset of void coalescence (Vishwakarma and Keralavarma, 2019) suggests a straightforward method for determining the flow stress in the coalescence band $\bar{\sigma}_b$ at the onset of instability, as follows.

The onset of coalescence corresponds to a bifurcation from diffuse to localized plasticity at the microscale. Hence, both the pre- and the post-localization yield criteria, Eqs. (25) and (6) respectively, must be simultaneously satisfied at the transition. Since the equivalent stress σ_{eq} equals the material flow stress $\bar{\sigma}$ given by Eq.(26), the only unknown quantity in (6) is the flow stress in the coalescence band $\bar{\sigma}_b$, which must, in general, be obtained by iterative solution of Eq.(6). However, the argument of the 'cosh' function in (6) is smaller than unity, except for very large values of the triaxiality ($T > \sim 4$), which fall outside the range of interest. Hence, an approximate closed form expression for $\bar{\sigma}_b$ is

obtained by neglecting the fourth and higher order terms in the Taylor series expansion of the 'cosh' function, leading to

$$\bar{\sigma}_b \approx \frac{\sqrt{3c_{\mathrm{sh}}^2 + f_b\beta^2 c_{\mathrm{n}}^2}}{1 - f_b}\bar{\sigma} \tag{27}$$

Note that the value of $\bar{\sigma}_b$ obtained above depends on the loading history through its dependence on f (via f_b), whose rate of evolution is history dependent as specified below.

2.3.3. Porosity evolution

The rate of evolution of the porosity f can be written as the sum of the nucleation rate of new voids and the rate of growth of existing voids; i.e.

$$\dot{f} = \dot{f}_{\mathrm{nuc}} + \dot{f}_{\mathrm{gr}} \tag{28}$$

Phenomenological models are frequently used to model void nucleation, such as the model proposed by Chu and Needleman (1980), which assumes a statistical distribution of second phase particles of varying nucleation strengths. Here, a pre-existing population of voids is assumed and void nucleation is disregarded.

The rate of growth of existing voids depends on the loading path, and can be related to the hydrostatic part of the plastic deformation rate obtained from porous plasticity models, due to plastic incompressibility of the matrix. Void growth is driven by the hydrostatic component of the stress, and is hence primarily sensitive to the triaxiality T. An approximate expression for $\dot{f}_{\mathrm{gr}}$ obtained using the classical Gurson (1977) model has the form (Pineau et al., 2016)

$$\dot{f}_{\mathrm{gr}} = \frac{3}{2}qf \sinh\left(\frac{3}{2}T\right)\dot{\varepsilon}_{\mathrm{eq}}^{p} \tag{29}$$

where q is a heuristic parameter introduced by Tvergaard (1982) to improve the correspondence between the predictions of the Gurson model and axisymmetric cell model simulations for the void growth rates. Assuming dilute porosities, second and higher order terms in f have been neglected in the derivation of the above equation.

Besides its primary dependence on T, recent studies have shown that $\dot{f}_{\mathrm{gr}}$ has a secondary, intrinsic dependence on the Lode parameter L (Benallal et al., 2014; Leblond and Morin, 2014). More significantly, there is an apparent effect of L due to induced anisotropy (void shape changes resulting from finite deformations). This apparent effect dominates over the intrinsic one and must be accounted for in some approximate way when using an isotropic model. By definition, the value of L falls in the range $[-1, 1]$, where $L = -1$ represents axisymmetric tensile stress states (uniaxial tension with superposed hydrostatic stress), $L = 0$ represents generalized shear (pure shear with superposed hydrostatic stress) and $L = 1$ represents axisymmetric compression (uniaxial compression with superposed hydrostatic stress). Three dimensional voided cell simulations suggest that the void growth rates for loading paths close to axisymmetric compression ($L = 1$) are significantly smaller compared to other loading paths at fixed T (see e.g. Vishwakarma and Keralavarma, 2019, Fig.4b). On the other hand, the porosity rates in the cell model simulations exhibit relatively small variations in the range from $L = -1$ to 0.

Based on the above observations from several cell model studies, a heuristic Lode dependent correction is proposed for the void growth law, which reads

$$\dot{f}_{\text{gr}} = f\left[\frac{3}{2}q\sinh\left(\frac{3}{2}T\right) - c\mathcal{H}(L)L^3\right]\dot{\varepsilon^p_{\text{eq}}} \tag{30}$$

where $\mathcal{H}(\cdot)$ denotes the Heaviside step function, and c is a positive constant that quantifies the Lode parameter's influence on void growth. The Lode dependent correction is effective only for positive values of L, and significant only for stress states close to $L = 1$ due to the cubic power of L. Moreover, as will be discussed in context below, the Lode dependence in the porosity rate equation is not as important as the Lode dependence implied by the coalescence equations (6)–(9), although both couple through the failure criterion (23).

3. Model Assessment

Unless otherwise noted, the values of the two heuristic parameters in the void growth law (30) are chosen as $q = 1.25$ and $c = 1$ in the results to be presented. On the other hand, we emphasize that failure criterion (23) does not contain any parameters beyond those used to describe plastic flow.

3.1. Fracture locus

For the special case of proportional loading, the values of the triaxiality T and the Lode parameter L remain constant throughout the loading history. In this case, the strain to failure $\varepsilon^f_{\text{eq}}$, defined as the value of $\varepsilon^p_{\text{eq}}$ at failure, is a function of T and L, and can be used as a measure of the material's intrinsic ductility. The equation $\varepsilon^f_{\text{eq}} = \varepsilon^f_{\text{eq}}(T, L)$ is often referred to in the literature as the equation of the fracture locus. The porosity can be determined as a function of the equivalent plastic strain by integrating Eq.(29), yielding:

$$f(\varepsilon^p_{\text{eq}}) = f_0 \exp\left\{\left[\frac{3}{2}q\sinh\left(\frac{3}{2}T\right) - c\mathcal{H}(L)L^3\right]\varepsilon^p_{\text{eq}}\right\} \tag{31}$$

where f_0 is the value of f at $\varepsilon^p_{\text{eq}} = 0$. Failure occurs when $\varepsilon^p_{\text{eq}} = \varepsilon^f_{\text{eq}}$ and $f(\varepsilon^f_{\text{eq}})$ satisfies the condition

$$\mathcal{C}(T, L, f(\varepsilon^f_{\text{eq}})) = 0 \tag{32}$$

which defines an implicit equation for the fracture locus in mixed stress and plastic strain space.

For example, assuming an initial porosity $f_0 = 0.001$ and isotropic hardening in $(26)_1$ defined through:

$$\bar{\sigma} = \sigma_0\left(1 + \frac{\varepsilon^p_{\text{eq}}}{\varepsilon_0}\right)^n \tag{33}$$

where σ_0 is the initial yield stress, ε_0 a reference plastic strain and n the strain hardening exponent, Eq.(32) is solved to obtain $\varepsilon^f_{\text{eq}}(T, L)$ for a range of values of T and L. Resulting plots of the failure loci in T-L-$\varepsilon^f_{\text{eq}}$ space are shown in Fig. 2 for two values of the hardening exponent.

For a nearly ideally plastic material ($n = 0.01$) the predicted strain to failure decreases rapidly with increasing triaxiality T, irrespective of the value of L, Fig. 2(a). The effect of the Lode parameter L is small compared to that of the triaxiality towards large values

(a)

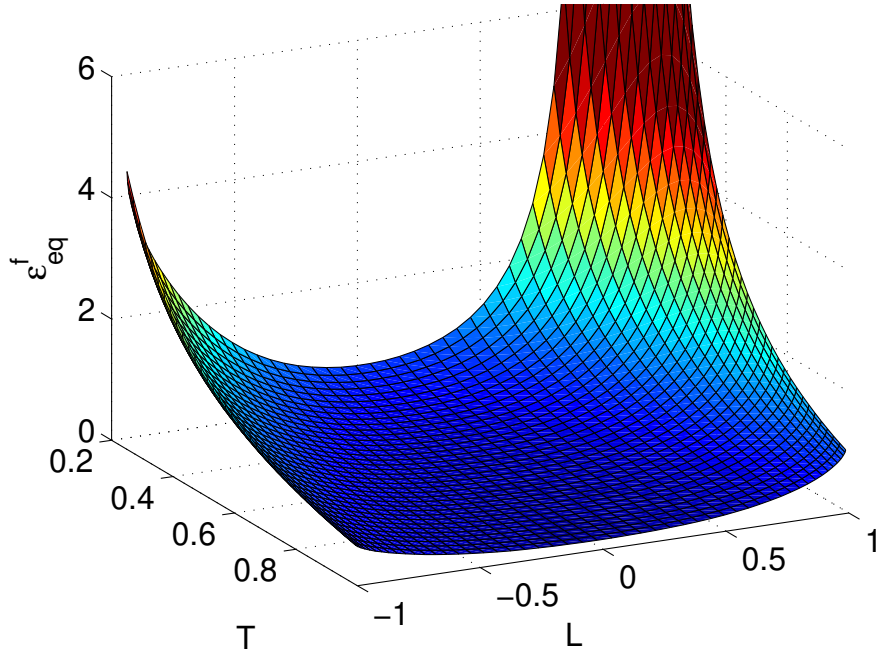

(b)

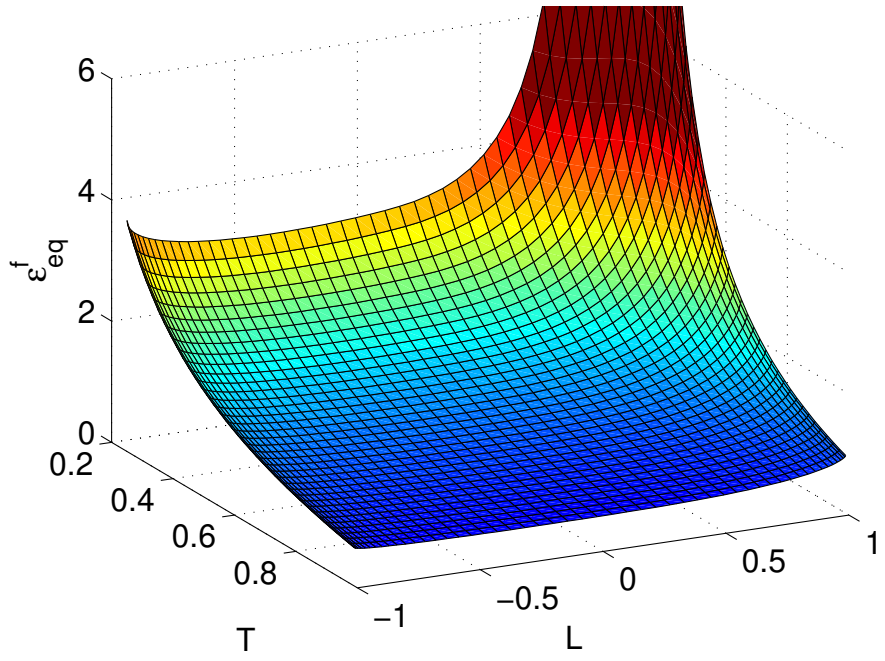

Figure 2: Three-dimensional fracture loci in the space of triaxiality T, Lode parameter L, and the equivalent strain to failure $\varepsilon^f_{\text{eq}}$, under proportional loading and for a power law hardening material with $\sigma_0 = 420$ MPa, $\varepsilon_0 = 0.002$, and hardening exponent (a) $n = 0.01$ (b) $n = 0.1$, in Eq. (33).

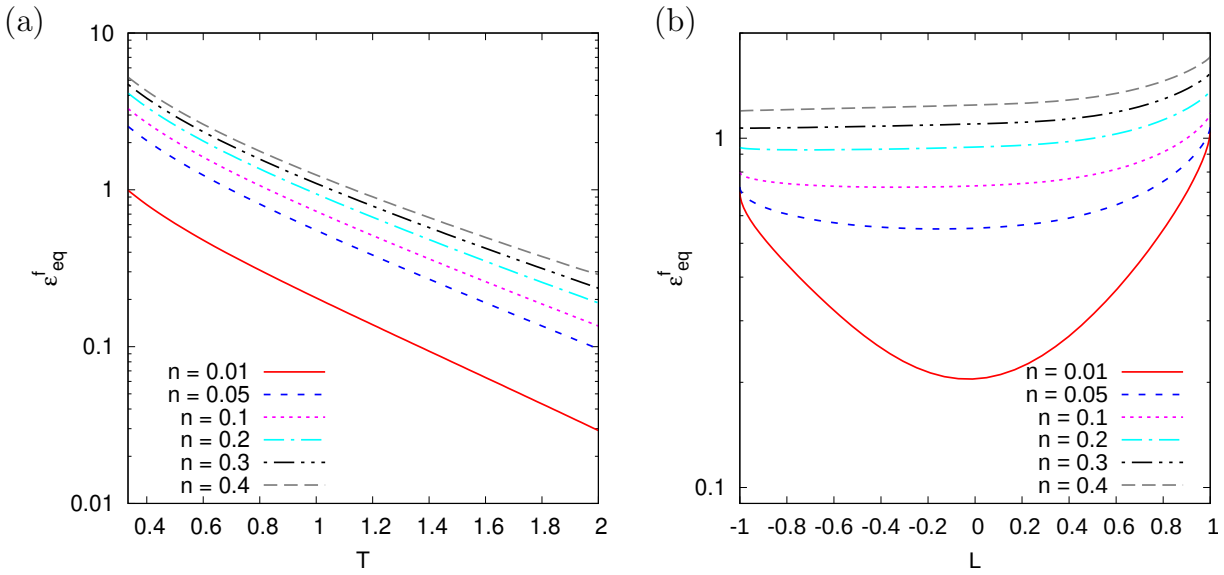

Figure 3: Variation of the strain to failure $\varepsilon^f_{\text{eq}}$ as a function of (a) T for constant $L = 0$ and (b) L for constant $T = 1$, for several representative values of the strain hardening exponent n.

of T. However, for low to moderate values of $T \leq 1$, the strain to failure exhibits a characteristic convex non-monotonic dependence on the Lode parameter, with significantly lower ductilities predicted under shear dominated loading paths with $|L| \ll 1$ compared to axisymmetric paths with $|L| \sim 1$. Recall that the void growth law (30) is independent of L in the range $L \in [-1, 0]$; indicating that the reduction in ductility for shear dominated loadings compared to axisymmetric tensile loadings ($L = -1$) is solely due to the Lode dependence of the failure criterion, Eq.(23). Importantly, the above result suggests that the shear induced damage effect and reduction in ductility observed in some experiments could be attributed to the Lode dependence of the failure criterion.

The fracture locus for a material with moderate strain hardening capacity $n = 0.1$ is shown in Fig. 2(b). Notice that the strains to failure under shear dominated loading paths with $|L| \ll 1$ are significantly larger than in the case $n = 0.01$, while the failure strains for axisymmetric loading paths show relatively little variation with n. This indicates that failure under shear dominated loading is primarily determined by the localization criterion (23), which depends strongly on strain hardening through the terms $H(\varepsilon^p_{\text{eq}})$ and $\bar{\sigma}_b$. Conversely, failure under axisymmetric loading paths appears to be primarily determined by void growth, Eq.(30), with a relatively smaller influence of n through the localization criterion. Fig. 2(b) also exhibits a convex variation of $\varepsilon^f_{\text{eq}}$ with L at fixed T as in Fig. 2(b), although the Lode effect on the strain to failure is small, except close to axisymmetric compressive loading paths with $L = 1$, even at low triaxialities.

The effect of strain hardening on ductility is further illustrated in Fig. 3, which shows the variation of the strain to failure $\varepsilon^f_{\text{eq}}$ as a function of T and L for several values of the hardening exponent n in the common range $0 < n < 0.5$. Fig. 3(a) shows the variation of $\varepsilon^f_{\text{eq}}$ as a function of T for generalized shear loadings with $L = 0$ and various values of n. Note that the variation of $\varepsilon^f_{\text{eq}}$ with T is nearly linear on the semi-log scale irrespective of the value of n, which indicates that the ductility decreases exponentially with increasing T, as observed in classical experiments (Pineau et al., 2016).

On the other hand, the variation of the ductility with L at fixed $T = 1$ in Fig. 3(b) is

non-monotonic, with a minimum in ductility predicted for some value of L in the range $-1 < L < 0$ for low to moderate values of the hardening exponent. This is a consequence of the fact that inhomogeneous yielding tends to occur at small plastic strain levels for shear dominated loading paths, which is associated with a sharp increase in the damage growth rate (Reddi et al., 2019). Therefore, in the absence of significant strain hardening, which stabilizes plastic flow, the instability criterion is satisfied at relatively small plastic strains for shear dominated loading paths. Although not perceptible for values of $n \geq 0.2$, a non-monotonic variation of $\varepsilon^f_{\text{eq}}$ with L is predicted for values of n as large as 0.3 in Fig. 3(b). The results in Fig. 3 also show that the ductility increases monotonically with the value of the hardening exponent, irrespective of the loading path, although the effect of n is most significant for shear dominated loading paths with $|L| \ll 1$.

3.2. Comparison with cell model simulations

The predictive capability of the failure criterion (23), and the uncoupled model formulated in Section 2.3, is now assessed against two recent sets of three dimensional finite-element cell model simulations by Vishwakarma and Keralavarma (2019) and Dunand and Mohr (2014). In this type of model, pioneered by Tvergaard (1982) and Koplik and Needleman (1988), a periodic cell, usually containing a single void in an elasto-plastic matrix, is subjected to a prescribed loading path until failure occurs by plastic collapse of the ligaments separating the voids, marking the onset of coalescence. Mesoscopic (cell level) measures of stress and strain rate are obtained by volume averaging the corresponding microscopic quantities in the cell:

$$\boldsymbol{\sigma} = \langle \boldsymbol{\sigma}_{\text{mic}} \rangle, \quad \mathbf{d}^e = \langle \mathbf{d}^e_{\text{mic}} \rangle, \quad \mathbf{d}^p = \langle \mathbf{d}^p_{\text{mic}} \rangle \tag{34}$$

where $\langle \cdot \rangle$ denotes the volume average over the cell, and the subscript 'mic' refers to microscopic quantities. For a cell subjected to periodic boundary conditions, the mesoscopic stress $\boldsymbol{\sigma}$ and deformation rate $\mathbf{d} = \mathbf{d}^e + \mathbf{d}^p$ are power conjugate quantities. The mesoscopic equivalent stress and strain measures are then defined in the usual way as indicated in Section 2.3.1.

It is important to mention here that void coalescence, as observed in cell model analysis using a single voided unit cell, corresponds to a deformation mode akin to that illustrated in Fig. 1(b), which is different from strain localization in the macroscopic sense. However, given the rapid softening associated with the onset of coalescence observed in the cell model studies for most loading paths, it is expected that macroscopic localization will occur shortly after the onset of coalescence. Hence, it is reasonable to compare the failure strain predicted using an instability based criterion such as (23) to the strain to coalescence observed in cell model studies, under the assumption that the latter represents an accurate lower bound estimate of the former.

First, we assess the model against the simulations of Vishwakarma and Keralavarma (2019) who considered a power law hardening material with the flow stress $\bar{\sigma}$ given by Eq.(33) using $\sigma_0 = 420$ MPa, $\varepsilon_0 = 0.002$ and $n = 0.1$ or $n = 0.01$. The loading parameters were varied in the ranges $T \in [\frac{2}{3}, 3]$ and $L \in [-1, 1]$. Other parameters were the initial void volume fraction $f_0 = 0.001$, Young's modulus $E = 210$ GPa and Poisson's ratio $\nu = 0.3$. These authors have also considered two cell aspect ratios, $\alpha = 1$ (cubic cell) and $\alpha = 2$ (tetragonal cell). The cubic cell was used only for axisymmetric loadings. For general triaxial loadings, when void coalescence occurs under combined tension and shear of the ligaments, the tetragonal cell is typically used (Tvergaard, 2009; Barsoum and

Faleskog, 2011; Dunand and Mohr, 2014). The choice of a tetragonal cell with sufficiently large α ensures that coalescence occurs in layers along the (short) transverse ligaments of the unit cell; and avoids practical difficulties in the detection of the onset of coalescence, especially under loading paths where a cubic cell shows a propensity of localization along multiple directions, such as $L = 0$ (multiple symmetric shear bands) or $L = 1$ (coalescence in layers or columns).

The range of failure strains obtained in the above-mentioned ranges of T and L is quite broad. Thus, for clarity, the results are shown in Fig. 4 for low to moderate stress triaxialities and in Fig. 5 for moderate to high stress triaxialities. All results pertain to $\alpha = 2$ to facilitate comparison with generalized shear ($L = 0$) and axisymmetric compression ($L = 1$) loading paths. In the cell simulation (solid lines), the strain to failure is determined by the onset of coalescence by plastic collapse of the ligaments, which is marked by $\times$; see Vishwakarma and Keralavarma (2019) for details of the method used to detect the onset of coalescence. In the uncoupled model (dotted lines), the ductility is limited by failure criterion (23), as marked by an open circle in figures 4 and 5.

The salient features of the cell simulations are as follows. For axisymmetric tensile loadings ($L = -1$), the equivalent stress drops abruptly beyond the onset of coalescence, Fig. 4(a), so that the strain to coalescence is a reasonable measure of intrinsic ductility. The onset of coalescence also coincides with an increase in the rate of porosity growth as observed in Fig. 4(b). For states of generalized shear ($L = 0$), plastic collapse ($\times$ marks) occurs at roughly the same strain levels as in the $L = -1$ case[2]; but the subsequent softening is more gradual, Fig. 4(c). Finally, for axisymmetric compressive stress states ($L = 1$), Figs. 4(e,f), the ductilities are significantly larger than the other two cases. Also, the transition to inhomogeneous flow is accompanied neither with an abrupt stress drop nor an acceleration in porosity growth. This effect has been highlighted as early as the works of Gologanu et al. (2001) and Benzerga and Besson (2001). The behavior at high triaxialities in Fig. 5 is qualitatively similar to Fig. 4, albeit the failure strains are much smaller.

Now, we turn to the analytical model predictions. By definition, the uncoupled model does not predict any softening in the effective response. The potential limitations of this will be discussed further below. An immediate consequence, however, is that the stress–strain response is independent of T and L. On the other hand, the porosity depends on the loading parameters thanks to Eq. (30). The value of the Tvergaard parameter $q = 1.25$ in (30) is chosen such that the predicted porosity rates for axisymmetric tensile loading paths approximately match the cell model simulations over a broad range of values of T. The chosen value of q is in fact the same as in an earlier similar study by Koplik and Needleman (1988). Notice that the same value of q also leads to a reasonable agreement for the porosity rates at $L = 0$ with the cell model simulations, justifying the assumption in Eq.(30) that void growth is Lode independent for negative values of L. The value of the second heuristic parameter $c = 1$ is chosen such that the reduction in void growth rates predicted by Eq.(30) for axisymmetric compression ($L = 1$) approximately matches the cell model simulations over the same range of T.

Note that, in addition to T, L and f, the failure criterion of Eq.(23) depends on the

[2]except at $T = 2/3$ for which the ductility is lower in shear, a trend that is exacerbated at low hardening capacity of the matrix.

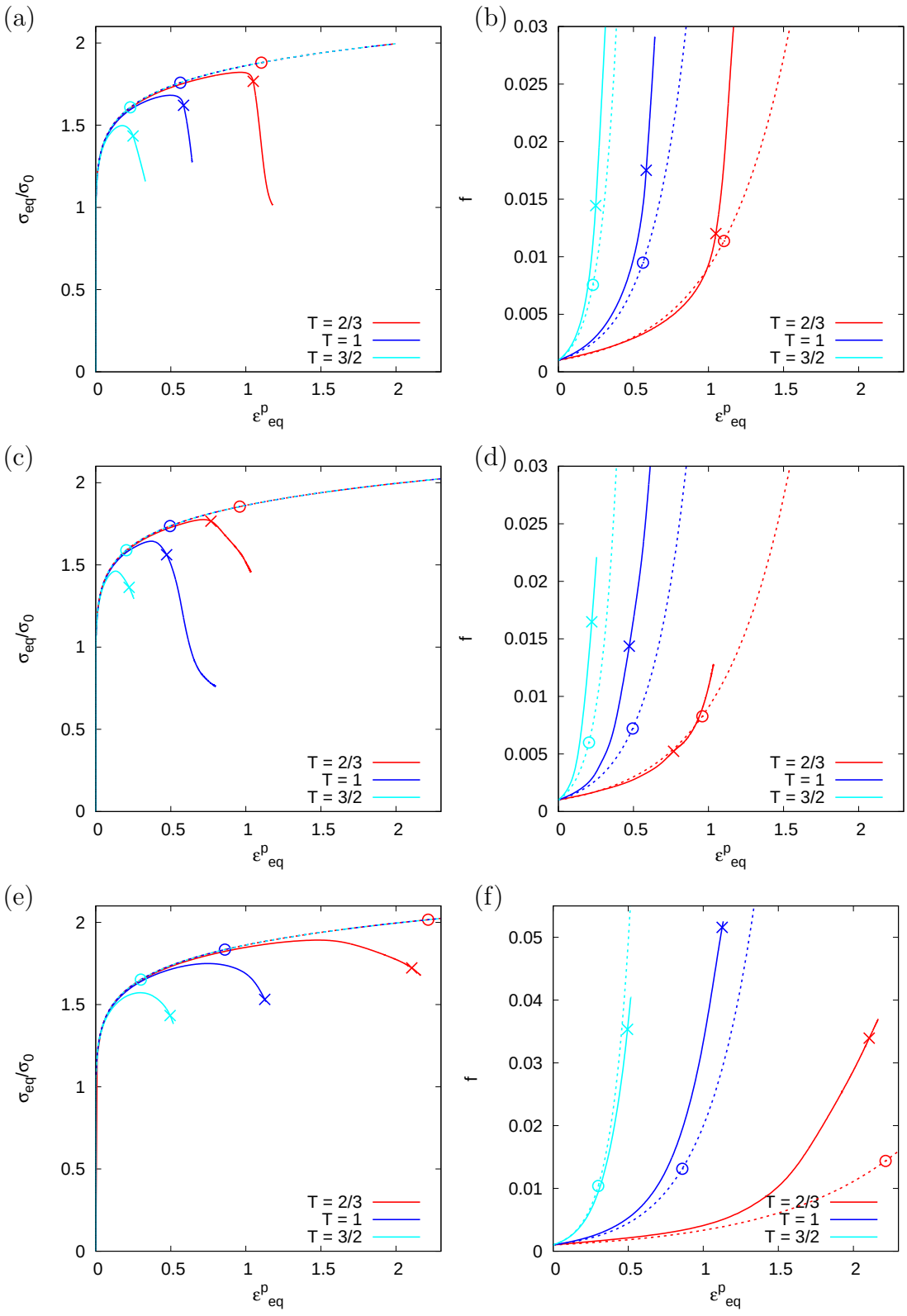

Figure 4: Comparison of the effective response of porous cells obtained from the cell model simulations of Vishwakarma and Keralavarma (2019) (solid lines) and the uncoupled model (dotted lines) for moderate values of the triaxiality T. Equivalent stress vs. strain: (a) $L = -1$ (c) $L = 0$ and (e) $L = 1$. Porosity vs. equivalent strain: (b) $L = -1$ (d) $L = 0$ and (f) $L = 1$. The $\times$ marks indicate the onset of coalescence in the cell model simulations, and the open circles mark the failure strains predicted by Eq.(23) in the uncoupled model.

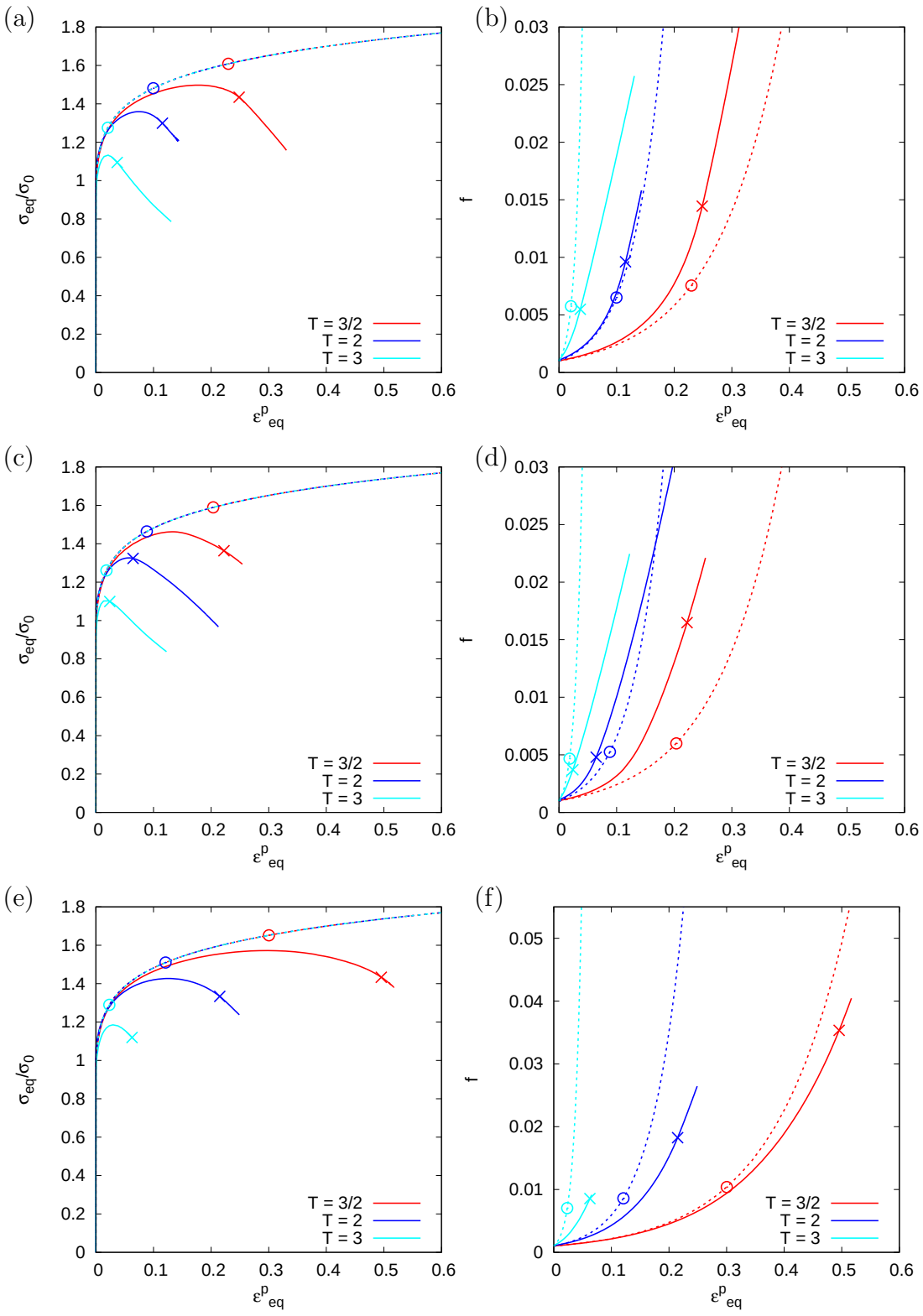

Figure 5: Comparison of the effective response of porous cells obtained from the cell model simulations of Vishwakarma and Keralavarma (2019) (solid lines) and the uncoupled model (dotted lines) for high values of the triaxiality T. Equivalent stress vs. strain: (a) $L = -1$ (c) $L = 0$ and (e) $L = 1$. Porosity vs. equivalent strain: (b) $L = -1$ (d) $L = 0$ and (f) $L = 1$. The $\times$ marks indicate the onset of coalescence in the cell model simulations, and the open circles mark the failure strains predicted by Eq.(23) in the uncoupled model.

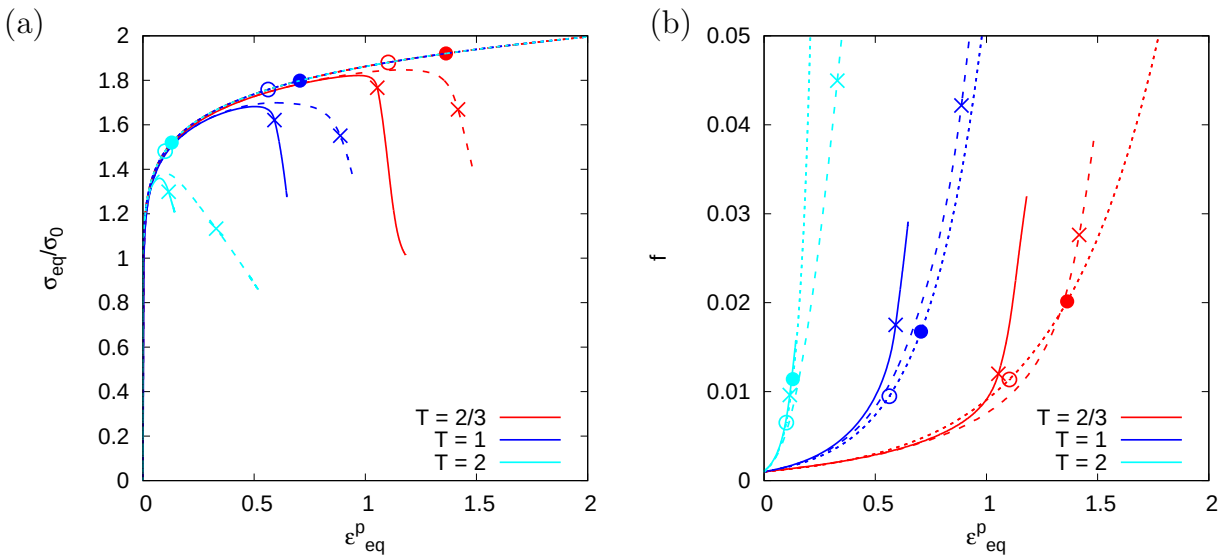

Figure 6: Comparison of the effective response of porous cells subjected to axisymmetric tensile loading ($L = -1$) obtained from the cell model simulations of Vishwakarma and Keralavarma (2019) for cell aspect ratios $\alpha = 2$ (solid lines) $\alpha = 1$ (dashed lines) and the uncoupled model (dotted lines): (a) equivalent stress vs. strain, and (b) porosity vs. equivalent strain. The $\times$ marks indicate the onset of coalescence in the cell model simulations, and the open and filled circles mark the failure strains predicted by Eq.(23) for $\alpha = 2$ and $\alpha = 1$, respectively.

porosity in the coalescence band f_b, which can be approximately related to the porosity f as $f_b = f^{2/3}$ in a statistically isotropic material containing a random distribution of voids. However, for a tetragonal lattice with cell aspect ratio $\alpha = 2$, coalescence always occurs along the close packed direction of voids due to the smaller initial ligament thicknesses. Assuming that the thickness of the coalescence band scales with the size of the voids, this leads to the relation (Vishwakarma and Keralavarma, 2019)

$$f_b = (2f)^{2/3} \tag{35}$$

The remaining equations in Section 2 remain unchanged irrespective of the distribution of the voids. The predicted failure strains using the uncoupled model are shown using the open circles in Figs. 4-5. It is clear that the model predictions are in good quantitative agreement with the triaxiality dependence of the coalescence strains observed in the cell model simulations, although the ductility is underestimated for axisymmetric compression ($L = 1$) for $T > 1$. In fact, failure strains predicted by the instability criterion for axisymmetric compression are in closer agreement with the maximum in the true stress-strain response rather than the onset of coalescence in the cell model simulations. This could be partially due to the choice of the cell aspect ratio $\alpha = 2$, which effectively prevents the occurrence of coalescence in columns.

The effect of the cell aspect ratio is now examined for the case $L = -1$ (axisymmetric tension), for which cell model results are available for both cubic ($\alpha = 1$) and tetragonal ($\alpha = 2$) distributions of voids. Fig. 6 compares the equivalent stress-strain and porosity growth curves for $\alpha = 2$ (solid lines) and $\alpha = 1$ (dashed lines). As is known from earlier cell model studies, the effective response is independent of void distribution at small plastic strain and porosity levels; although the cell aspect ratio has a significant influence on the onset of coalescence marked by the $\times$ symbols. Irrespective of the triaxiality, coalescence occurs earlier for $\alpha = 2$ compared to $\alpha = 1$ due to the smaller initial

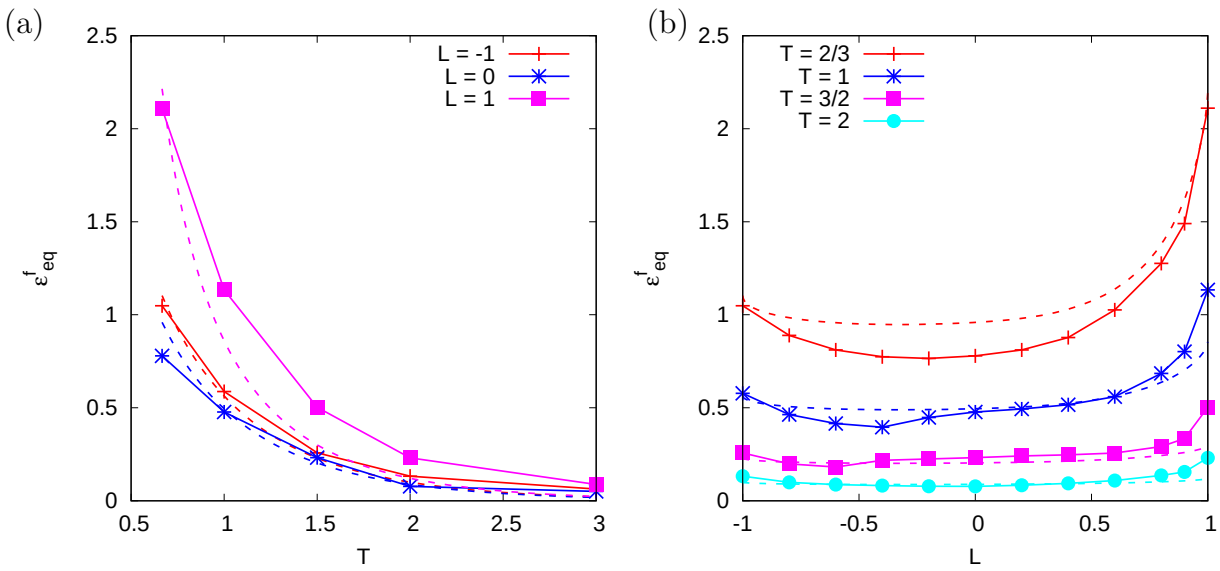

Figure 7: Strain to failure $\varepsilon^f_{\text{eq}}$ versus (a) the stress triaxiality T, and (b) Lode parameter L, obtained from the cell model simulations of Vishwakarma and Keralavarma (2019) (points) and the uncoupled model (dashed lines) for $f_0 = 0.001$ and a power law hardening material with $n = 0.1$.

ligament thicknesses along the transverse direction of the unit cell. The uncoupled model predictions are shown using dotted lines in Fig. 6, where the strains to failure are marked by the open circles for $\alpha = 2$ and filled circles for $\alpha = 1$. The uncoupled model captures the effect of void distribution on the strains to failure, although there is an apparently significant quantitative discrepancy with the cell model results for the case $T = 2$. Further investigation shows that the localization indicator for $T = 2$ and $\alpha = 1$ showed significant oscillations and a tendency towards localization at lower plastic strains (see Vishwakarma and Keralavarma, 2019, Fig.3c), closer to the prediction from the uncoupled model, although the *ad hoc* critical value of the localization indicator was only attained later. As mentioned previously, detection of the onset of coalescence turns out to be more difficult for the case of the cubic void distribution, which is the reason for adopting the tetragonal cell aspect ratio in the recent 3D cell model studies. All the fracture loci shown in the rest of this paper are obtained for $\alpha = 2$.

Fig. 7(a) shows cross-sections of the failure locus in the plane of the triaxiality T and the strain to failure $\varepsilon^f_{\text{eq}}$ for the three values of L examined in Figs. 4 and 5. On the other hand, Fig. 7(b) shows cross-sections of the same failure locus in the L–$\varepsilon^f_{\text{eq}}$ plane for various values of T. Note that intermediate values of L are used, which were not included in previous plots. The equivalent strains to the onset of coalescence in the cell model simulations are shown using line-points, while the dashed lines show predictions from the uncoupled model. All the curves in Figs. 7(a,b) are characteristic of the same "material" for which $f_0 = 0.001$ and $n = 0.1$. The qualitative as well as quantitative variation of the strain to failure with T and L is well reproduced by the model. In particular, the uncoupled model captures the exponential decrease of the ductility with T irrespective of the value of L, the relatively minor effect of L on the strains to failure in the range $-1 \leq L \leq 0$, and the significant increase in ductility for $L = 1$ towards lower values of T.

As discussed previously, the strain to failure is determined by the competition between strain hardening in the matrix and the softening due to void growth in the coalescence band, as quantified by the first and second terms, respectively, in Eq.(23). As such,

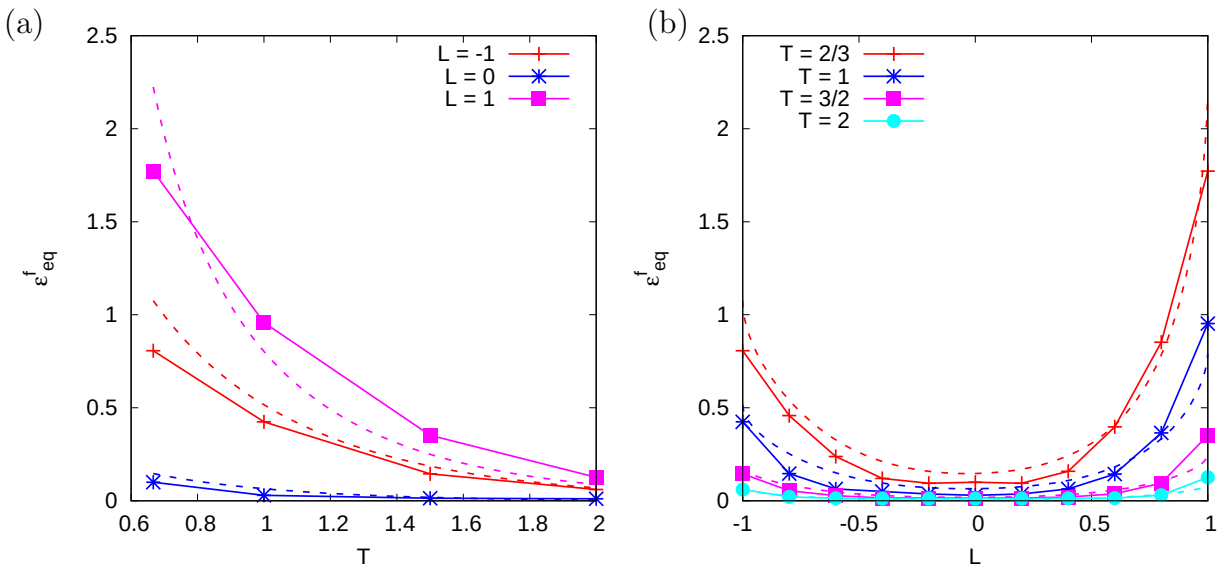

Figure 8: Strain to failure $\varepsilon^f_{\text{eq}}$ versus (a) the stress triaxiality T, and (b) Lode parameter L, obtained from the cell model simulations of Vishwakarma and Keralavarma (2019) (points) and the uncoupled model (dashed lines) for $f_0 = 0.001$ and a power law hardening material with $n = 0.01$.

the strain hardening behavior of the matrix has a significant influence on the ductility predictions obtained using the uncoupled model (c.f. Fig. 2). The simulated and predicted failure loci, projected onto the T-$\varepsilon^f_{\text{eq}}$ and L-$\varepsilon^f_{\text{eq}}$ planes, are compared in Figs. 8(a) and (b) respectively, for a very low strain hardening capacity $n = 0.01$. The reduced strain hardening capacity has a dramatic effect on the ductility under generalized shear loading conditions, with significantly lower strains to failure predicted for loading paths with $|L| \ll 1$ compared to axisymmetric loading paths, irrespective of the value of T. This is a consequence of the fact that porous microstructures favor early strain localization under generalized shear loading paths. In the absence of significant strain hardening, which stabilizes plastic flow, strain localization in the ligaments occurs at very small plastic strains, consistent with the cell model simulations. Note that the predicted values of the strain to failure using the uncoupled model are again in good quantitative agreement with the results of cell model simulations.

Next, we assess the model against the simulations of Dunand and Mohr (2014) who considered lower triaxialities in the range $0.2 \leq T \leq 1$ and a Voce-like saturation strain hardening model for the matrix, specified in rate form as

$$\bar{\sigma}(\varepsilon^p_{\text{eq}} = 0) = \sigma_0, \quad H(\varepsilon^p_{\text{eq}}) = H_0 \left(1 - \frac{\bar{\sigma}}{\sigma_\infty}\right)^r \tag{36}$$

where $H(\varepsilon^p_{\text{eq}}) = \frac{\partial \bar{\sigma}}{\partial \varepsilon^p_{\text{eq}}}$ is the instantaneous hardening rate. The material parameters were $E = 185$ GPa, $\nu = 0.3$, $\sigma_0 = 450$ MPa, $\sigma_\infty = 1.2$ GPa, $H_0 = 20$ GPa and $r = 2$. These authors also considered a tetragonal cell with $\alpha = 2$ and initial porosity $f_0 = 0.007$. In addition, they accounted for the deformation induced rotation of the principal axes of the void, by ensuring that the orientation of the principal axes of the void remains fixed relative to the principal axes of loading.

Fig. 9 shows the comparison between the strains to failure obtained from the cell model simulations of Dunand and Mohr (2014), and the uncoupled model based on criterion (23)

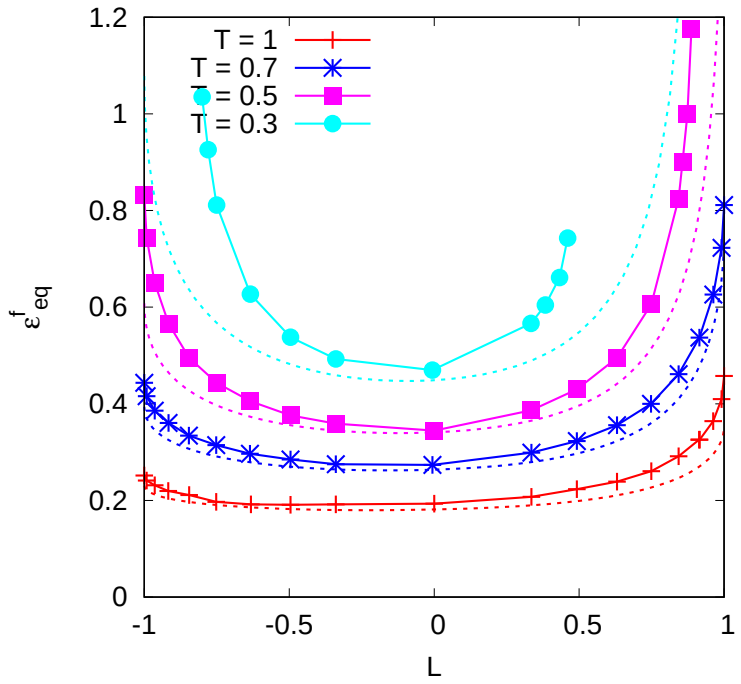

Figure 9: Comparison between the cell model simulations of Dunand and Mohr (2014) for the strain to failure $\varepsilon^f_{\text{eq}}$ as a function of the Lode parameter L for several values of the stress triaxiality $T \leq 1$ (line-points) and predictions from the uncoupled model (dashed lines). The initial porosity was $f_0 = 0.007$ and strain hardening in the matrix is given by Eq.(36).

supplemented with the pre-coalescence Mises plasticity model, the band hardening equation (36) and the porosity growth law (30). The comparison is depicted in the plane of strain to failure versus Lode parameter. The model predictions are in good quantitative agreement with the Lode dependence of the ductility observed in the cell model results for values of $T \geq 0.5$. However, for a low value of $T = 0.3$ (close to uniaxial tension), the model appears to significantly underestimate the ductility towards axisymmetric loading paths with $|L| \sim 1$. This is most probably a consequence of induced anisotropy due to void shape evolution, whose effect becomes much more significant at low triaxiality levels when porosity growth is slow.

Axisymmetric cell model simulations indicate that under uniaxial tension with $T = 1/3$, significant void distortion occurs, although the porosity growth rate is negligible; and void coalescence does not occur up to very large strains, consistent with the results in Fig. 9. Based on this observation, Thomas et al. (2016) have proposed a modification of the void growth law of the form

$$\dot{f} = \kappa f \sinh\left[\kappa\left(T - 1/3\right)\right]\dot{\varepsilon}^p_{\text{eq}} \tag{37}$$

where the limiting value of the parameter $\kappa \approx \sqrt{3}$ for highly prolate spheroidal voids, obtained from void shape dependent models, is to be used at low triaxialities. However, the above modification entails that the damage growth rate asymptotes to zero at $T = 1/3$ irrespective of the value of the Lode parameter. On the other hand, the results of Fig. 9 show that the predicted strains to failure using damage law (30) remain accurate for shear dominated loading paths with $|L| \ll 1$, even for triaxialities as low as $T = 0.3$. This result essentially points to the limits of applicability of isotropic models in predicting fracture at low triaxialities.

To further illustrate this point, consider some limit cases of the failure criterion (23). Note that the terms $-\frac{\partial \mathcal{F}^C}{\partial \bar{\sigma}_b}$, $\frac{\partial \mathcal{F}^C}{\partial f}$ and Q_p in (23) are always positive, while H and Q_f can have either sign. For a non-hardening or softening matrix ($H \leq 0$), localization is predicted at the onset of inhomogeneous loading if $Q_f \geq 0$. On the other hand, if damage growth is negative or zero ($Q_f \leq 0$), localization never occurs if the matrix exhibits positive strain hardening ($H > 0$). This limitation of the model results from the assumption of isotropy (neglect of void shape changes), and failure is not predicted under certain low triaxiality loading paths such as pure shear or uniaxial compression. Anisotropic models that accurately capture void shape effects on damage growth are needed to predict failure under low triaxiality ($T \leq 1/3$) loading paths such as pure shear (see Torki and Benzerga, 2018), which is outside the scope of the present paper.

4. Discussion

Several issues are now addressed, which concern the basis of the uncoupled model, its suitability for engineering practice, the insights it provides on the failure of ductile solids, and its domain of validity.

4.1. Strain localization versus void coalescence

The concept of ductile failure as a plastic instability is not new. It has been the prevalent view ever since the Gurson model (1977) and Rice's localization theory (1976) have concurrently emerged as potent frameworks for analyzing ductile fracture. The rationale is that porosity-induced strain softening can lead to loss of ellipticity of the incremental problem in rate-independent plasticity. Furthermore, most cell model studies to date exhibit a maximum in the true stress long before the onset of void coalescence by micro-scale flow localization. The intrinsic softening thus leaves the possibility wide open for a macroscopic instability to set an effective limit on ductility. Examples of localization analyses that employed constitutive relations for porous plastic solids go back to Yamamoto (1978); Needleman and Rice (1978); Ohno and Hutchinson (1984); Perrin (1992); Ponte Castañeda and Zaidman (1994); Rousselier (1991) and more recently Danas and Ponte Castañeda (2012); Morin et al. (2019).

The key question is: what is the most appropriate structure of the porous material's constitutive relation to be used in a localization analysis of this sort? For the sake of discussion, it is both useful and necessary to adopt the recently introduced terminology of homogeneous yielding for void-growth dominated plasticity versus inhomogeneous yielding for either void-coalescence dominated plasticity or void-distortion under shear-dominated loadings (Torki and Benzerga, 2018). The viewpoint underlying the recent development of porous material plasticity models (see Keralavarma and Chockalingam 2016; Torki et al. 2015 and references therein) is that a constitutive relation that accounts *a priori* for the potential competition between homogeneous yielding and inhomogeneous yielding is necessary to settle some of the outstanding issues in ductile fracture modeling. In particular, whether ductility is limited by plastic instability or by void impingement can only be ascertained when a suitable framework of this sort is available.

An obvious, albeit non-trivial, alternative to the above line of investigations is to not rely on any constitutive description of the behavior of a porous material, and explore fully computational solutions. Direct numerical simulations of this kind are still not accessible

enough to draw unequivocal conclusions. In order to discriminate mesoscale inhomogeneous yielding from macroscopic plastic instabilities (shear bands), such simulations need to involve many voids and be three-dimensional while exploring the space of remote stress states. An effort in this direction has recently been attempted by Tekoğlu et al. (2015) who carried out an imperfection band analysis, and hence did not address the competition between inhomogeneous yielding and strain localization. Instead, they examined how early the onset of void coalescence would occur after macroscopic strain localization. They found that the outcome depends on stress triaxiality, and this rather curious result seems to be rooted in their *ad hoc* definition of the onset of void coalescence.

Another outstanding issue is that of what role, if any, does a nonuniform void distribution play on the effective response of a porous plastic solid and, by way of consequence, on the aforementioned competition between plastic instability and failure by void impingement. In spite of numerous previous attempts at tackling this issue, it is fair to say that it remains largely unsettled. Notwithstanding this difficulty, it is likely that nonuniform void distributions would have a negligibly small effect on homogeneous yielding and a potentially large effect on inhomogeneous yielding (see the appendix of Benzerga 2002). This in itself hints at the need for the recently developed line of inhomogeneous yielding models.

In this paper, failure by plastic instability has been investigated using an isotropic, multi-surface porous plasticity model. In doing so, we have also used recent results by Vishwakarma and Keralavarma (2019) who have shown that Rice's localization condition is actually not met until inhomogeneous yielding sets in. This was shown under various loading programs in terms of driving stress triaxiality and Lode parameter values. This result has fundamental consequences in light of the above discussion, and ought to be re-examined when void distribution effects can be studied. The result also has a profound practical importance, especially since the strain at the onset of plastic instability as well as the orientation of the localization plane were both found to be close to their microscopic counterparts at the onset of coalescence. This aspect has been taken advantage of here, in developing a triaxiality and Lode parameter dependent failure criterion.

4.2. Structure of failure criterion

The development of failure criteria that are simple enough to be widely adopted in engineering practice has value. A key question relates to the structure of the said failure criterion. A recent line of models seems to have accepted that a critical strain criterion is the format by default. Typically, a stress-based criterion is assumed, which is then transformed using the hardening law into a space of the failure strain $\varepsilon^f_{\rm eq}$, triaxiality T and the Lode parameter L (Bai and Wierzbicki, 2008; Dunand and Mohr, 2011). The validity of several assumptions underlying such transformations are little discussed and are much more constraining than may be thought.

Importantly, failure criteria based solely on attainment of a critical strain cannot account for the loading history dependence of damage growth, which is a strongly nonlinear function of the plastic strain as determined from experiments and micromechanical analysis. Hence, such models are restricted to proportional or nearly proportional loading histories; though such restrictions are rarely heeded in practice. Alternative criteria based on attainment of a critical value of the damage parameter, such as the porosity, coupled with a history dependent damage evolution law, can account for the loading path dependence. However, such models are also limited in their ability to account for the in-

fluence of the matrix plastic behavior, specifically the strain hardening law, on the critical conditions for failure. Damage growth models such as (30) are only weakly dependent on strain hardening through the pre-localization plasticity model. However, the strains to failure in the cell model simulations depend strongly on strain hardening, especially under shear dominated loading conditions (c.f. Figs. 7-8).

Instability based failure criteria, such as the one developed here, falls into neither of the above categories; and can account for the competition between strain hardening and void growth induced softening, which determines the critical conditions for failure in the cell model simulations. For the special case of proportional loading, the void growth law can be integrated in closed form to write the porosity as an explicit function of the total plastic strain, Eq.(31); and the failure criterion can be expressed in the space of $\varepsilon^f_{\rm eq}$, T and L, analogous to the critical strain models; see Eq.(32).

The importance of performing the instability analysis on a plasticity model that accounts for *inhomogeneous* yielding at the microscale can be seen by examining the results of Danas and Ponte Castañeda (2012), who performed a similar localization analysis using a void shape dependent plasticity model assuming diffuse yielding at the microscale. Their conclusion was that void shape evolution leads to a monotonic reduction in ductility as a function of L from -1 to 1, and that strain hardening in the matrix had little influence on the strain at which loss of ellipticity is predicted. Both the above conclusions are contrary to the results of cell model simulations, indicating that it is essential to account for inhomogeneous yielding at the mesoscale prior to carrying out a localization analysis.

4.3. Origin of stress-state dependence

A major advantage of failure criterion (23) over phenomenological criteria is its micromechanical basis. It thus enables the stress-state dependence to be analyzed for both the intrinsic fracture locus as well as, in time, of apparent fracture loci, as accessed in laboratory experiments.

There are two distinct but related causes for the Lode dependence of the limit strain. The first lies in the growth of damage, as embodied in the modified porosity evolution equation (30). When all is accounted for, this contribution is relatively small, parameterized and not fully intrinsic.

That the effect of L on porosity growth is small can be seen in two ways. For a frozen microstructure, constrained to remain isotropic, refined analyses of Gurson's hollow sphere problem show that the effect of L on the effective yield surface is secondary relative to that of T (Leblond and Morin, 2014; Benallal et al., 2014). On the other hand, in actual evolution problems, as in cell model analyses, the cumulated effect remains small for $-1 \leq L \leq 0$ and may become noticeable when L approaches 1; see Fig. 4 of Vishwakarma and Keralavarma (2019). However, the latter effect is mostly due to induced anisotropy so that any interpretation based on L would be ill-founded.

Thus, any significant effect of L on porosity growth is apparent, not intrinsic, and manifests through void shape evolution effects. In order to account for this, within the confines of an isotropic model, equation (30) introduces a Lode dependent term, which aims at capturing the slow-down in void growth for L nearing 1. One consequence is that equation (30) must be parameterized to represent a more complex situation where induced anisotropy affects the outcome.

At this juncture, it is appropriate to compare the proposed evolution law (30) with that introduced by Nahshon and Hutchinson (2008). First, in our formulation, the damage

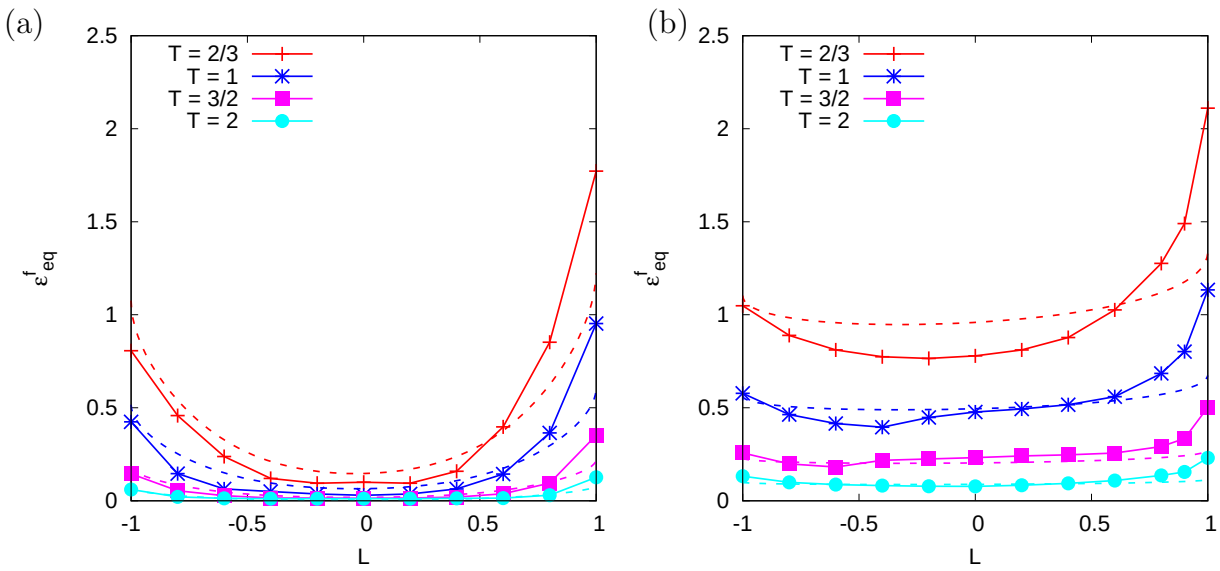

Figure 10: Comparison of the fracture loci in the L–$\varepsilon^f_{\rm eq}$ plane predicted by the uncoupled model using a Lode independent void growth law, Eq.(30) with $c = 0$, with the cell model simulation results of Vishwakarma and Keralavarma (2019) for a power law hardening material with (a) $n = 0.01$ and (b) $n = 0.1$.

variable f still has the physical meaning of a void volume fraction. This is not the case in their model. Second, Nahshon and Hutchinson (2008) assume that damage grows faster under shear states. This is inconsistent with cell model simulations. It should also be noted that in their model all Lode dependence enters through the evolution equation of the damage variable, whereas in the present model the proposed modification underlying Eq. (30) is secondary, as will become evident below.

The second origin of the Lode dependence of ductile failure is rooted in the nature of the limiting event: localization of plastic flow in a band whose orientation is determined by the major and minor principal stresses. Given that the band is generally oriented close to 45° between the maximum and minimum principal directions, the critical condition for localization depends strongly on the relative magnitude of the shear stresses, or the Lode parameter, in addition to the porosity and the instantaneous strain hardening rate in the band. This contribution is embodied in failure criterion (23). It is large, not parameterized and intrinsic. This is the most important insight gained from the present analysis.

In order to fully appreciate this, one must first notice that the heuristic modification of $\dot{f}$ through Eq. (30) couples through the failure criterion (23). To apportion both contributions, the fracture loci may be re-evaluated using $c = 0$ in Eq. (30), that is using a Lode-independent porosity evolution law. The resulting predictions are compared with the cell model simulation results in Fig. 10. The only noticeable degradation in the predictions occurs for Lode parameter values near 1; as expected since L does not affect the rate of porosity growth for $L < 0$ in the new law. In particular, the important effect of strain hardening is captured regardless of the correction underlying Eq. (30).

The fracture loci predicted by the instability model (Figs. 7,8) are cross-sections of general loci, as illustrated in Fig. 2. In particular, the strain to failure is found to be a monotonically decreasing function of T for $T > 1/3$, irrespective of the value of L. In fact, the model predicts such a trend over a wider range $T > 0$ with an asymptote

at $T = 0$. This is an artefact of neglecting anisotropic effects. If a mechanism were to prevail in, say simple shear ($T = 0$, $L = 0$), so that a *finite* shear strain to failure can be rationalized, then the failure locus could exhibit a non-monotonic trend with respect to T over a wider range $T \geq 0$. Such a mechanism is, however, inherently anisotropic (Torki and Benzerga, 2018) and the proportional fracture locus would exhibit a discontinuity at $T = 1/3$ (Torki, 2019). Such an inherently non-monotonic fracture locus should not be conflated with apparent trends in experimental tests limited to plane stress loading (Bai and Wierzbicki, 2008). Indeed, when such loci are shown as $\varepsilon^f_{\rm eq}$ versus T, it must be noted that the Lode parameter L is *not* kept constant. In addition, plane stress failure is often mediated by shear bands, in which case the strain to failure is highly sensitive to boundary conditions, not just the overall stress state.

4.4. Domain of validity

The simple uncoupled model developed here is applicable within a range of conditions and under the assumption that the mechanism driving failure is void-mediated. With this in mind, the model is not to be used without caution if (i) there is significant initial or induced anisotropy; or (ii) failure is due to macroscopic strain localization requiring multi-void analyses.

For simplicity, the model assumes isotropic damage growth and neglects void shape effects, because of which it significantly underestimates the ductility under axisymmetric loading paths at low T, such as uniaxial tension. Correcting for the above within an isotropic framework requires additional phenomenological correction of the void growth law beyond the Lode dependent second term in Eq.(30). While the modification proposed by Thomas et al. (2016) is a step in this direction, the model developed here is not suitable for prediction of ductile failure under very low triaxiality, say $T \leq 1/3$.

The model also assumes isotropy in the distribution of voids, and requires correction when microstructural features deem failure by void coalescence more likely along certain directions than others. This is straightforward only when the direction of coalescence is known *a priori*, as in the case of the tetragonal void distribution assumed in the cell model studies. Often, void coalescence involves a few voids, e.g. at a crack tip, in which case the local arrangement of voids implies anisotropic response. In principle, the uncoupled approach adopted here can be generalized to account for anisotropic microstructures, at the expense of simplicity.

5. Conclusion

A micromechanics-based constitutive relation for porous plastic solids is used together with a plastic instability criterion to develop a stress state dependent criterion for ductile failure. Along with a damage-free plasticity model and a Lode-dependent, uncoupled model of void growth, it is demonstrated that the new model can quantitatively predict the strains to failure obtained from voided cell simulations over a wide range of loading paths and strain hardening properties.

- The failure criterion depends on the stress triaxiality T and the Lode parameter L, in addition to the porosity and the strain hardening behavior of the material. The T and L dependence appears through the normal and shear stresses on the plane of localization, whose normal is assumed to lie in the plane defined by the major and minor principal stresses.

- The functional form for the failure criterion is obtained by combining an isotropic version of the void coalescence criterion of Keralavarma and Chockalingam (2016) together with the plastic instability criterion of Rice (1976). The final form of the criterion, Eq.(23), clearly shows that failure occurs as a result of the competition between the strain hardening and void growth induced softening inside the coalescence band.

- A Lode-dependent correction is proposed for the void growth law obtained from the Gurson model. Under proportional loading, the void growth law can be integrated to write the porosity as a function of the plastic strain, which is then used to derive an implicit equation for the failure locus in the mixed space of T, L and the equivalent strain to failure $\varepsilon_{\text{eq}}^{f}$.

- The proposed model is shown to yield quantitative accurate predictions for the strains to failure obtained from voided cell simulations, for moderate to large values of T and a wide range of values of L, as a function of the strain hardening parameters of the material.

- The proposed model can be further extended by adopting a coupled approach whereby the Gurson model is used as a pre-localization constitutive relation. When induced anisotropy effects are important, such as under simple shear, anisotropic multisurface models may be employed.

Acknowledgments

SMK acknowledges financial support from Indira Gandhi Centre for Atomic Research, Kalpakkam, through the IITM-IGCAR cell. AAB gratefully acknowledges financial support from the National Science Foundation under grant CMMI-1932975.

References

References

Bai, Y., Wierzbicki, T., 2008. A new model of metal plasticity and fracture with pressure and lode dependence. Int. J. Plasticity 24 (6), 1071–1096.

Barsoum, I., Faleskog, J., 2011. Micromechanical analysis on the influence of the lode parameter on void growth and coalescence. Int. J. Solids Struct. 48 (6), 925–938.

Benallal, A., Desmorat, R., Fournage, M., 2014. An assessment of the role of the third stress invariant in the gurson approach for ductile fracture. Eur. J. Mech. 47, 400–414.

Benzerga, A. A., 2002. Micromechanics of Coalescence in Ductile Fracture. J. Mech. Phys. Solids 50, 1331–1362.

Benzerga, A. A., Besson, J., 2001. Plastic potentials for anisotropic porous solids. Eur. J. Mech. 20 (3), 397–434.

Benzerga, A. A., Leblond, J. B., 2010. Ductile fracture by void growth to coalescence. Adv. Appl. Mech. 44, 169–305.

Benzerga, A. A., Leblond, J.-B., 2014. Effective Yield Criterion Accounting for Microvoid Coalescence. J. App. Mech. 81, 031009.

Benzerga, A. A., Thomas, N., Herrington, J. S., 2019. Plastic flow anisotropy drives shear fracture. Scientific Rep. 9, Art. No. 1425.

Beremin, F. M., 1981. Experimental and numerical study of the different stages in ductile rupture: application to crack initiation and stable crack growth. In: Nemat-Nasser, S. (Ed.), Three-Dimensional Constitutive relations of Damage and Fracture. Pergamon press, pp. 157–172.

Chu, C., Needleman, A., 1980. Void nucleation effects in biaxially stretched sheets. J. Eng. Mat. Tech. 102, 249–256.

Danas, K., Ponte Castañeda, P., 2012. Influence of the lode parameter and the stress triaxiality on the failure of elasto-plastic porous materials. Int. J. Solids Struct. 49 (11), 1325–1342.

Dunand, M., Mohr, D., 2011. On the predictive capabilities of the shear modified gurson and the modified mohr-coulomb fracture models over a wide range of stress triaxialities and lode angles. J. Mech. Phys. Solids 59, 1374–1394.

Dunand, M., Mohr, D., 2014. Effect of lode parameter on plastic flow localization after proportional loading at low stress triaxialities. J. Mech. Phys. Solids 66, 133–153.

Gologanu, M., Leblond, J.-B., Perrin, G., Devaux, J., 2001. Theoretical models for void coalescence in porous ductile solids – II: Coalescence in "columns". Int. J. Solids Struct. 38, 5595–5604.

Gurson, A. L., 1977. Continuum Theory of Ductile Rupture by Void Nucleation and Growth: Part I– Yield Criteria and Flow Rules for Porous Ductile Media. J. Eng. Mat. Tech. 99, 2–15.

Johnson, G. R., Cook, W. H., 1985. Fracture characteristics of three metals subjected to various strains, strain rates, temperatures and pressures. Eng. Frac. Mech. 21 (1), 31–48.

Keralavarma, S. M., 2017. A multi-surface plasticity model for ductile fracture simulations. J. Mech. Phys. Solids 103, 100–120.

Keralavarma, S. M., Chockalingam, S., 2016. A criterion for void coalescence in anisotropic ductile materials. Int. J. Plasticity 82, 159–176.

Koplik, J., Needleman, A., 1988. Void growth and coalescence in porous plastic solids. Int. J. Solids Struct. 24 (8), 835–853.

Leblond, J.-B., Morin, L., 2014. Gurson's criterion and its derivation revisited. J. App. Mech. 81, 051012.

Madou, K., Leblond, J.-B., 2012. A Gurson-type criterion for porous ductile solids containing arbitrary ellipsoidal voids–I: Limit-analysis of some representative cell. J. Mech. Phys. Solids 60, 1020–1036.

Morin, D., Daehli, L. E., Borvik, T., Benallal, A., Hopperstad, O. S., 2019. Numerical study of ductile failure under non-proportional loading. Eur. J. Mech. 74, 221–241.

Morin, L., Leblond, J.-B., Benzerga, A. A., Kondo, D., 2016. A unified criterion for the growth and coalescence of microvoids. J. Mech. Phys. Solids 97, 19–36.

Nahshon, K., Hutchinson, J. W., 2008. Modification of the Gurson Model for shear failure. Eur. J. Mech. 27, 1–17.

Needleman, A., Rice, J. R., 1978. Limits to ductility set by plastic flow localization. In: Koistinen, D. P. (Ed.), Mechanics of sheet metal forming. Plenum, pp. 237–267.

Ohno, N., Hutchinson, J. W., 1984. Plastic Flow Localization Due to Non-Uniform Void Distribution. J. Mech. Phys. Solids 32 (1), 63–85.

Perrin, G., 1992. Contribution à l'étude théorique et numérique de la rupture ductile des métaux. Ph.D. thesis, Ecole Polytechnique.

Pineau, A., Benzerga, A. A., Pardoen, T., 2016. Failure of metals I: Brittle and ductile fracture. Acta Mater. 107, 424–483.

Ponte Castañeda, P., Zaidman, M., 1994. Constitutive models for porous materials with evolving microstructure. J. Mech. Phys. Solids 42, 1459–1495.

Reddi, D., Areej, V. K., Keralavarma, S. M., 2019. Ductile failure simulations using a multi-surface coupled damage-plasticity model. Int. J. Plasticity.

Rice, J., 1976. The localization of plastic deformation. In: Koiter, W. (Ed.), 14th int. cong. Theoretical and Applied Mechanics. North–Holland, Amsterdam, pp. 207–220.

Rice, J. R., Tracey, D. M., 1969. On the enlargement of voids in triaxial stress fields. J. Mech. Phys. Solids 17, 201–217.

Rousselier, G., 1991. Application of a linear perturbation stability analysis to strain localization in plastic dilatant materials with strain-softening. C. R. Acad. Sci. Paris 313, 1367–1373.

Rudnicki, J. W., Rice, J. R., 1975. Conditions for the localization of deformation in pressure–sensitive dilatant materials. J. Mech. Phys. Solids 23, 371–394.

Tekoğlu, C., Hutchinson, J. W., Pardoen, T., 2015. On localization and void coalescence as a precursor to ductile fracture. Philosophical Transactions of the Royal Society of London A: Mathematical, Physical and Engineering Sciences 373, 20140121.

Thomas, N., Basu, S., Benzerga, A. A., 2016. On fracture loci of ductile materials under non-proportional loading. Int. J. Mech. Sci. 117, 135–151.

Torki, M. E., 2019. Ductile Fracture under Combined Tension and Shear: Theory and Applications. Ph.D. thesis, Texas A&M University, USA.

Torki, M. E., Benzerga, A. A., 2018. A mechanism of failure in shear bands. Extreme Mechanics Letters 23, 67–71.

Torki, M. E., Benzerga, A. A., Leblond, J.-B., 2015. On void coalescence under combined tension and shear. J. App. Mech. 82, 071005.

Tvergaard, V., 1982. On localization in ductile materials containing spherical voids. Int. J. Frac. 18, 237–252.

Tvergaard, V., 2009. Behaviour of voids in a shear field. Int. J. Frac. 158, 41–49.

Vishwakarma, V., Keralavarma, S. M., 2019. Micromechanical modeling and simulation of the loading path dependence of ductile failure by void growth to coalescence. Int. J. Solids Struct.

Yamamoto, H., 1978. Conditions for shear localization in the ductile fracture of void–containing materials. Int. J. Frac. 14, 347–365.